

Combined Use of Monte Carlo DNA Damage Simulations and Deterministic Repair Models to Examine Putative Mechanisms of Cell Killing

David J. Carlson,^{a,b} Robert D. Stewart,^{a,1} Vladimir A. Semenenko^{a,c} and George A. Sandison^a

^a School of Health Sciences, Purdue University, West Lafayette, Indiana; ^b Department of Radiation Oncology, Stanford University School of Medicine, Stanford, California; and ^c Department of Radiation Oncology, Medical College of Wisconsin, Milwaukee, Wisconsin

Carlson, D. J., Stewart, R. D., Semenenko, V. A. and Sandison, G. A. Combined Use of Monte Carlo DNA Damage Simulations and Deterministic Repair Models to Examine Putative Mechanisms of Cell Killing. *Radiat. Res.* 169, 447–459 (2008).

A kinetic repair-misrepair-fixation (RMF) model is developed to better link double-strand break (DSB) induction to reproductive cell death. Formulas linking linear-quadratic (LQ) model radiosensitivity parameters to DSB induction and repair explicitly account for the contribution to cell killing of unrejoinable DSBs, misrepaired and fixed DSBs, and exchanges formed through intra- and intertrack DSB interactions. Information from Monte Carlo simulations is used to determine the initial yields and complexity of DSBs formed by low- and high-LET radiations. Our analysis of published survival data for human kidney cells suggests that intratrack DSB interactions are negligible for low-LET radiations but increase rapidly with increasing LET. The analysis suggests that no class of DSB is intrinsically unrejoinable or that DSB reparability is not strictly determined by the number of lesions forming the DSB. For radiations with LET >110 keV/μm, the model predicts that the relative cell killing efficiency, per unit absorbed dose, should continue to increase, whereas data from published experiments indicate a reduced cell killing efficiency. This observation suggests that the Monte Carlo simulation overestimates the DSB yield beyond 110 keV/μm or that other biological phenomena not included in the model, such as proximity effects, are important. For 200–250 kVp X rays (~1.9 keV/μm), only about 1% of the one-track killing is attributed to intratrack binary misrepair interactions. The analysis indicates that the remaining 99% of the lethal damage is due to other types of one-track damage, including possible unreparable, misrepaired and fixed damage. Compared to the analysis of the X-ray results, 48% of the one-track lethal damage caused by 5.1 MeV α particles (~88 keV/μm) is due to intratrack DSB interactions while the remainder is due to other forms of one-track damage. © 2008 by Radiation Research Society

INTRODUCTION

The observation that the biological effectiveness of radiation, per unit absorbed dose, varies with radiation quality provides useful clues about the nature of the initiating events and mechanisms underlying the responses of cells and tissues to radiation. For example, experiments with repair-proficient mammalian cells have shown that the relative biological effectiveness (RBE) for cell killing tends to increase with increasing linear energy transfer (LET) up to about 100–200 keV/μm and then starts to decrease (1–6). The peak in the RBE curve occurs when the average distance between adjacent energy deposits is approximately the same as the diameter of the DNA double helix (~2 nm), which in turn provides circumstantial evidence that radiation damage to DNA is positively correlated to cell killing. The decrease in RBE above 100–200 keV/μm presumably occurs because the deposition of additional energy within the same DNA segment is less effective at producing lethal damage per unit absorbed dose.

Mutant *xrs5* cells derived from wild-type Chinese hamster ovary (CHO) cells have a reduced capacity for double-strand break (DSB) repair, and these cells exhibit a constant RBE for carbon ions with an LET below 100 keV/μm (7). From 100 to 480 keV/μm, RBE decreases monotonically as the LET of the carbon ion increases (7). The survival response of human fibroblasts (180BR) and CHO cells (*xrs6*) deficient in non-homologous end joining (NHEJ) is also the same for X rays and 70 keV/μm carbon ions (8). The 180BR human fibroblasts are a DNA ligase IV mutant, and *xrs6* cells are a Ku80 mutant. These and many other studies (9–11) all suggest that the induction and repair of DNA damage plays a vital role in the survival response of cells to particles of varying radiation quality.

The relationship of RBE to particle LET is complex and, in general, depends on the biological end point of interest. For end points such as DSB induction and cell survival, RBE tends to increase as the particle LET increases up to about 100 to 200 keV/μm and then reaches a plateau or even decreases [e.g., see refs. (5, 12, 13)]. The observation that trends in DSB induction and cell killing are similar for

¹ Address for correspondence: Purdue University School of Health Sciences, 550 Stadium Mall Drive, West Lafayette, IN 47907-2051; e-mail: trebor@purdue.edu.

radiations of very different quality provides useful opportunities to test hypotheses regarding the potential mechanisms linking DSB induction and processing to cell killing. Several possible mechanisms may contribute to the increased RBE of high-LET radiations. For example, if some forms of clustered damage, such as complex DSBs, are intrinsically unrejoinable and lethal, the RBE for cell killing will increase as the LET increases because the initial yield of complex damage tends to increase with increasing LET (14–16). A second hypothesis is that LET effects arise because the initial DSB yield ($\text{Gy}^{-1} \text{ cell}^{-1}$) increases with increasing LET, and a random subset of the initial DSBs are misrepaired or become unrejoinable because of physiochemical damage fixation processes or incomplete repair. Pairs of DSBs formed by the same or different tracks can also interact with each other to form lethal and nonlethal exchanges, i.e., the intra- and intertrack pairwise DSB interactions, also known as binary misrepair (17, 18). Pairwise DSB interactions may increase with increasing LET because of proximity effects (19) and because the overall DSB yield tends to increase with increasing LET.

In this article, a kinetic repair-misrepair-fixation (RMF) model is developed to better link DSB induction and processing to reproductive cell death. The linear-quadratic (LQ) survival model is shown to be an approximate time-integrated solution to the RMF. LQ radiosensitivity parameters are derived from survival data for human kidney T-1 cells exposed to ionizing radiation of increasing particle LET. The derived parameter estimates are used to investigate some of the putative mechanisms relating DSB induction and processing to radiation sensitivity. A novel aspect of the reported studies is that the results of Monte Carlo simulations for the induction of DNA damage (16) are used to examine the potential reparability of simple and complex DSBs and to assess the possible contribution to cell killing of intra- and intertrack binary misrepair without introducing an inordinate number of purely adjustable biological parameters into the modeling process.

REPAIR-MISREPAIR-FIXATION (RMF) MODEL

Exchange-type chromosome aberrations result from the incorrect rejoining of break ends associated with two different DSBs, i.e., the breakage and reunion theory of chromosome aberration formation [reviewed in refs. (19, 20)]. *Intratrack* binary misrepair occurs when the spatially and temporally correlated energy deposits formed by one radiation track through a cell creates two or more DSBs that interact in pairwise fashion to form an exchange. In contrast, *intertrack* binary misrepair arises from the pairwise interaction of break ends associated with DSBs that were formed by two separate radiation tracks through a cell. DSBs formed by the same radiation track are effectively created at the same time and are, on average, more likely to interact in pairwise fashion than DSBs formed by different tracks that, depending on dose rate, may be separated

by large time intervals (e.g., minutes or hours). The probability that two DSBs interact in pairwise fashion decreases as the time between DSB formation increases because one DSB may be rejoined before the second one is created. That is, two DSBs cannot interact in pairwise fashion if one DSB is repaired before the second one is created.

The mechanisms of action embodied in binary misrepair models, such as the repair-misrepair (RMR) model (17) and the lethal-potentially lethal (LPL) model (18), are broadly consistent with the breakage and reunion theory of chromosome aberration formation. Although the earlier RMR and LPL models provide a useful conceptual framework to link the conversion of sublethal damage (i.e., the DSB) into lethal and nonlethal exchanges through the intertrack binary misrepair process, their original formulation did not explicitly consider intratrack binary misrepair. The RMF model developed in this article combines concepts from the RMR and LPL models and considers intra- and intertrack binary misrepair. Explicit consideration of intra- and intertrack binary misrepair provides opportunities to explain and predict LET effects from first principles.

Induction of Rejoinable and Intrinsically Unrejoinable DSBs

Suppose that complex DSBs composed of j or more lesions (strand breaks, damaged bases or abasic sites) are intrinsically unrejoinable. That is, the presence of multiple lesions within the DSB suffices to permanently inhibit enzymatic processing or ligation of the break ends to their correct partner. Then the fraction of the initial DSBs that are potentially rejoinable is given by

$$f_R = \frac{1}{\Sigma} \sum_{i=2}^{j-1} \Sigma_i \quad (1)$$

Here Σ is the total number of DSBs $\text{Gy}^{-1} \text{ cell}^{-1}$ and Σ_i is the expected number of DSBs $\text{Gy}^{-1} \text{ cell}^{-1}$ composed of exactly i lesions. The summation in Eq. (1) is from $i = 2$ to $j - 1$ because all DSBs are composed of at least two strand breaks. Because Σ and Σ_i can be estimated using the Monte Carlo Damage Simulation (MCDS) algorithm (16), the only purely adjustable parameter in Eq. (1) is the value of j , which is an indicator of DSB complexity. The MCDS damage yields are modeled after more detailed track structure simulations by Nikjoo *et al.* (21) and Friedland *et al.* (22, 23). The MCDS model has been shown to correctly reproduce the local complexity of several forms of clustered DNA damage, including SSBs and DSBs (16, 24).

To model intratrack binary misrepair interactions, estimates of the expected number of potentially rejoinable DSBs *per track* are needed. The average number of potentially rejoinable DSBs formed per track is the product of the frequency-mean specific energy per radiation event (25), denoted \bar{z}_F , and the expected number of potentially rejoinable DSBs $\text{Gy}^{-1} \text{ cell}^{-1}$, i.e., $\bar{z}_F f_R \Sigma$. As a first approximation, the frequency-mean specific energy (in Gy) for a

spherical target composed of water with diameter d is given by (25)

$$\bar{z}_F = 0.204 \frac{\text{LET}}{d^2} \left(\frac{\text{keV}}{\mu\text{m}^3} \right). \quad (2)$$

This formula is derived under the assumption that charged particles randomly traverse the target in straight lines (i.e., no multiple scattering) and that energy losses occur according to the continuous-slowing-down approximation. For some combinations of site sizes and charged-particle types and energies, the assumptions may be strongly violated, and so the accuracy of Eq. (2) is poor. For example, multiple scattering increases the path length through the volume and hence energy deposition whereas δ -ray formation, bremsstrahlung and energy straggling may decrease the energy deposition to the volume (26).

Rate of Intra- and Intertrack Pairwise DSB Interaction

Let $p(L)$ denote the probability that exactly L rejoinable DSBs are induced in the nuclear DNA of a cell. The initial rate at which break ends associated with two different DSBs are incorrectly rejoined to each other is proportional to the product of the integral number of DSBs in the cell, L , and the number of DSBs minus one (an individual DSB cannot interact in pairwise fashion with itself), i.e., $\eta L(L - 1)$, where η is the probability per unit time that break ends interact in pairwise fashion. The expected rate of pairwise DSB rejoining is thus

$$\begin{aligned} \langle -\eta L(L - 1) \rangle &= -\eta \sum_L [L(L - 1)]p(L) \\ &= -\eta(\langle L^2 \rangle - \langle L \rangle), \end{aligned} \quad (3)$$

where $\langle L \rangle$ and $\langle L^2 \rangle$ are the first and second moments of the distribution of DSBs formed among a uniformly irradiated population of cells. The binary misrepair interaction rate therefore cannot be determined without knowledge of the second moment of the distribution of DSBs.

The initial distribution of DSBs among a uniformly irradiated population of cells can be modeled by a Neyman (compound binomial) distribution (27) with a variance equal to

$$\sigma^2 = n(n - 1)\delta\psi^2 + n\delta\psi. \quad (4)$$

Here δ is the average number of radiation tracks passing through the nucleus of a cell, n is the average number of times a radiation track crosses a DNA segment (e.g., a section of a chromosome a few tens or hundreds of base pairs in length), and ψ is the probability that a DSB occurs in the DNA segment after a particle crossing. The product $n\delta\psi$ represents the average number of DSBs $\text{Gy}^{-1} \text{ cell}^{-1}$, which is typically ~ 40 DSBs $\text{Gy}^{-1} \text{ cell}^{-1}$ for mammalian cells irradiated by low-LET radiation (14). Also, the average number of radiation tracks passing through the cell equals the absorbed dose divided by the frequency-mean specific energy (25), i.e., $\delta = D/\bar{z}_F$. In the limit when a

radiation track intersects a large number of DNA segments while passing through the cell nucleus (i.e., n becomes large), $n(n - 1) \cong n^2$ and the Neyman distribution reduces to a compound Poisson distribution with variance

$$\sigma^2 = n\delta\psi(1 + n\psi). \quad (5)$$

The product $n\psi = \bar{z}_F \Sigma$ represents the average number of DSBs formed *per track* through the nucleus. The expected number of potentially rejoinable DSBs per track is $f_R n\psi = f_R \bar{z}_F \Sigma$. Because the variance of a distribution equals the second moment of the distribution minus the square of the first moment, the second moment of the initial distribution of DSBs among a uniformly irradiated population of cells is $n\delta\psi(1 + n\psi) + (n\delta\psi)^2$. As a first approximation, we assume that the distribution of the number of rejoinable DSBs in a cell is proportional to the initial number of DSBs per cell, i.e., $\langle L \rangle \cong f_R n\delta\psi = f_R \Sigma D$, and that the second moment of the distribution of the number of potentially rejoinable DSBs per cell is $\langle L^2 \rangle \cong \delta f_R \bar{z}_F \Sigma (1 + f_R \bar{z}_F \Sigma) + (\delta f_R \bar{z}_F \Sigma)^2$. The right-hand side of Eq. (3) can now be expressed as

$$\begin{aligned} \langle -\eta L(L - 1) \rangle &\cong -\eta(n\delta\psi)(n\delta\psi + n\psi) \\ &= -\eta \langle L \rangle (\langle L \rangle + f_R \bar{z}_F \Sigma). \end{aligned} \quad (6)$$

In Eq. (6), the product $-\eta f_R \bar{z}_F \Sigma \langle L \rangle$ denotes intratrack pairwise DSB interaction, and $-\eta \langle L \rangle \langle L \rangle$ denotes intertrack pairwise DSB interactions. The minus sign indicates that both processes remove (rejoin) DSBs in the DNA. LET effects arise in Eq. (6) because Σ and \bar{z}_F tend to increase with increasing LET and the fraction of DSBs that are potentially rejoinable, f_R , tends to decrease with increasing LET. Trends in \bar{z}_F can be estimated using Eq. (2), and trends in f_R and Σ can be estimated using Monte Carlo simulations, e.g., the MCDS program (16).

Rates of DSB Induction, Processing and Conversion into Lethal Damage

For a population of cells uniformly irradiated at time t with absorbed dose rate $\dot{D}(t)$, the average number of potentially rejoinable DSBs produced in a cell during dt is $f_R \Sigma \dot{D}(t) dt$. Once formed, potentially rejoinable DSBs may be removed by first- or second-order repair processes and by damage fixation. To simplify the notation, the average number of DSBs in a cell, $\langle L \rangle$, will henceforth be denoted as L . The first-order DSB removal process is represented by $\lambda L(t)$, where the rate constant λ is the sum of the rates of DSB repair (λ_R) and damage fixation (λ_F). Intra- and intertrack binary misrepair are represented by $\eta f_R \bar{z}_F \Sigma L(t)$ and $\eta L^2(t)$, respectively. The expected rate of change in the average number of potentially rejoinable DSBs per cell at time t may now be expressed in terms of a balance (conservation of damage) equation, i.e.,

$$\frac{dL(t)}{dt} = f_R \Sigma \dot{D}(t) - (\lambda + \eta f_R \bar{z}_F \Sigma) L(t) - \eta L(t)L(t). \quad (7)$$

The RMF model considers five potential mechanisms for the conversion of DSBs into lethal forms of damage. The expected number of intrinsically unrejoinable, and thus lethal, DSBs (i.e., complex DSBs) formed in a cell during dt is $(1 - f_R)\Sigma\dot{D}(t) dt$. The lethal rejoining of a single DSB (linear misrepair) is $(1 - a)\varphi\lambda_R L(t)$, where $(1 - a)$ is the probability that a single DSB is misrepaired and φ is the probability that a misrepaired DSB is lethal. The fixation of DSBs by extrinsic processes is $\lambda_F L(t)$. The lethal misrejoining of two DSBs created by the same track is $\gamma\eta f_{R\bar{R}}\Sigma L(t)$, and the lethal misrejoining of DSBs created by two radiation tracks is $\gamma\eta L(t)L(t)$. Here a fraction $\gamma \sim 0.5$ of the exchanges formed through pairwise DSB interactions are lethal, i.e., approximately one lethal dicentric or centric ring is formed for each nonlethal translocation (28). Based on these considerations, the conversion of DSBs into lethal forms of damage in cells exposed to low- and high-LET radiation is described by the balance equation

$$\begin{aligned} \frac{dF(t)}{dt} = & (1 - f_R)\Sigma\dot{D}(t) + (\theta\lambda + \gamma\eta f_{R\bar{R}}\Sigma)L(t) \\ & + \gamma\eta L(t)L(t). \end{aligned} \quad (8)$$

Here $dF(t)/dt$ represents the expected rate of change in the average number of lethal forms of DNA damage per cell at time t and the fraction of DSBs that undergo lethal first-order misrepair and damage fixation is $\theta \equiv [(1 - a)\varphi\lambda_R + \lambda_F]/\lambda$.

The RMF model reduces to the original RMR model (17) for the special case when the rate of DSB fixation (λ_F) is zero, all DSBs are considered rejoinable (i.e., $f_R = 1$), and intratrack binary misrepair is negligible (i.e., $\eta f_{R\bar{R}}\Sigma \ll \lambda$). The RMF model reduces to the LPL model (18) for the special case when intratrack binary misrepair is negligible, the probability that a misrepaired DSB is lethal (φ) and the rate of DSB fixation (λ_F) is zero, and the fraction of lethal exchanges (γ) is unity. The main difference between the RMR and LPL is that (1) the LPL model assumes that a fraction $(1 - f_R)$ of the initial DSBs are intrinsically unrejoinable and lethal while neglecting the putative lethal misrepair pathway, i.e., a lethal damage term proportional to $L(t)$, and (2) the RMR model accounts for a lethal first-order misrepair pathway while neglecting the possibility that some damage may be intrinsically unrejoinable and lethal. Neither the RMR nor the LPL model includes the intratrack binary misrepair or damage fixation pathways included in the RMF model. Damage fixation is presumably a kinetic process, whereas intrinsically unrejoinable DSBs are formed immediately upon creation.

Linear-Quadratic (LQ) Survival Model as a Time-Integrated Solution of the RMF Model

In the limit of low doses and dose rates, the LQ model (29–31) can be derived from kinetic models, such as the RMR and LPL models, using perturbation theory and other methods (20, 32, 33). This is also true for the RMF model.

The α and β lethal damage coefficients for one- and two-track cell killing mechanisms can be formulated in terms of the DSB induction, rejoining and fixation parameters of the RMF model, such that²

$$\alpha = [1 - f_R(1 - \theta)]\Sigma + \kappa\bar{z}_F(f_R\Sigma)^2 \quad \text{and} \quad (9)$$

$$\beta = (\kappa/2)(f_R\Sigma)^2, \quad (10)$$

where $\kappa = [\eta/\lambda][\gamma - \theta]$ is the fraction of initial DSBs that undergo pairwise damage interaction. In the LQ model, the Lea-Catcheside dose protraction factor G (20) accounts for the effects of DSB repair and, for a single dose of radiation delivered at a constant dose rate during time interval T , is given by

$$G(\lambda, T) = \frac{2}{(\lambda T)^2}(e^{-\lambda T} + \lambda T - 1). \quad (11)$$

As long as the dose rate remains constant, the irradiation time will increase with increasing dose, which means that under this condition G decreases with increasing dose even though the dose rate remains constant. Even for high dose rates, dose protraction effects may have a significant impact on cell killing and, ultimately, treatment effectiveness (34).

METHODS AND MATERIALS

Survival Data for Human Kidney T-1 Cells Irradiated by X Rays and Selected Ions

Cell survival data sets for human kidney T-1 cells exposed *in vitro* to ionizing radiation of increasing particle LET are analyzed (1–4, 35). The Biosoft® Ungraph software is used to estimate the mean surviving fraction as a function of dose from the published figures. Estimates of radiosensitivity parameters for cells exposed to X rays (200–250 kVp) are derived from survival data reported by Barendsen *et al.* (1) and Barendsen and Walter (3). Survival data reported by Barendsen *et al.* (35), Barendsen (2) and Barendsen *et al.* (4) are used to derive radiosensitivity parameters for cells exposed to deuterons (${}^2\text{H}^+$) with kinetic energies from 3 MeV to 14.9 MeV (LET = 5.6–20 keV/ μm) and to α particles (${}^4\text{He}^{2+}$) with kinetic energies from 1.8 to 26.8 MeV (LET = 24.6–200 keV/ μm).

Nonlinear Regression Analysis

A standard approach to parameter estimation involves minimizing a positively weighted sum of the errors (34, 36). For a data set $(x_1, y_1), \dots, (x_n, y_n)$, let y_i denote the i th estimate of the surviving fraction for a given dose x_i and $f(x_i, \Omega)$ be the model-predicted surviving fraction for the same exposure conditions where Ω denotes the set of LQ parameters, e.g., α , β and τ (or λ), that can be adjusted to minimize a prescribed loss function. The following loss function is used to estimate parameters:

$$\chi = \sum_{i=1}^n [\ln y_i - \ln f(x_i, \Omega)]^2. \quad (12)$$

Here n is the total number of data points (absorbed dose values at which survival is evaluated). For *in vitro* cell survival data, point estimates of the LQ radiosensitivity parameters are obtained by minimizing Eq. (12) using a quasi-Newton, nonlinear optimization algorithm implemented in

² D. J. Carlson, Mechanisms of intrinsic radiation sensitivity: the effects of DNA damage repair, oxygen, and radiation quality. PhD Thesis, Purdue University, 2006 (<http://rh.healthsciences.purdue.edu/student/djcarlson/>).

TABLE 1
Estimates of LQ Radiosensitivity Parameters Derived from *In Vitro* Survival Data For Human Kidney T-1 Cells Irradiated with X Rays, Deuterons ($^2\text{H}^+$) or α Particles ($^4\text{He}^{2+}$)

Reference(s)	Radiation type	LET (keV/ μm)	Σ (DSBs Gy $^{-1}$ cell $^{-1}$)	\bar{z}_F (Gy)	α (Gy $^{-1}$)	$\beta \times 10^2$ (Gy $^{-2}$)
(1, 3)	200/250 kVp X rays	~ 1.9	50.08	0.0155	0.265 (0.238, 0.293)	2.65 (2.33, 2.90)
(4)	14.9 MeV $^2\text{H}^+$	5.6	58.26	0.0457	0.269 (0.112, 0.437)	2.91 (0.58, 5.15)
(35)	14.9 MeV $^2\text{H}^+$	5.6	58.26	0.0457	0.221 (0.113, 0.368)	5.09 (3.08, 6.45)
(35)	6.3 MeV $^2\text{H}^+$	11	68.23	0.0898	0.317 (0.209, 0.472)	4.99 (2.84, 7.54)
(35)	3.5 MeV $^2\text{H}^+$	17.4	80.23	0.1420	0.441 (0.340, 0.541)	3.22 (1.98, 4.82)
(4)	3 MeV $^2\text{H}^+$	20	83.95	0.1632	0.584 (0.502, 0.632)	0.38 (0.00, 2.29)
(35)	26.8 MeV $^4\text{He}^{2+}$	24.6	81.40	0.2007	0.640 (0.523, 0.766)	1.84 (0.00, 4.19)
(4)	25 MeV $^4\text{He}^{2+}$	26	83.04	0.2122	0.724 (0.478, 0.864)	0.94 (0.00, 6.51)
(4)	8.3 MeV $^4\text{He}^{2+}$	61	117.5	0.4978	1.188 (1.039, 1.331)	0.08 (0.00, 0.45)
(35)	8.3 MeV $^4\text{He}^{2+}$	61	117.5	0.4961	1.033 (0.876, 1.204)	5.45 (0.00, 11.7)
(35)	5.2 MeV $^4\text{He}^{2+}$	85.8	132.5	0.7001	1.545 (1.414, 1.616)	1.05 (0.00, 4.93)
(4)	5.1 MeV $^4\text{He}^{2+}$	88	133.4	0.7181	1.329 (1.012, 1.511)	3.00 (0.00, 21.2)
(4)	4 MeV $^4\text{He}^{2+}$	110	139.6	0.8976	1.776 (1.637, 1.845)	2.55 (0.00, 13.2)
(2)	4 MeV $^4\text{He}^{2+}$	110	139.6	0.8976	1.680 (1.421, 1.855)	2.10 (0.00, 17.1)
(2)†	3.6 MeV $^4\text{He}^{2+}$	123	142.8	1.0037	1.518 (1.448, 1.630)	0.00 —
(2)†	3.1 MeV $^4\text{He}^{2+}$	141	146.2	1.1506	1.625 (1.450, 1.781)	1.47 (0.00, 12.8)
(4)†	2.5 MeV $^4\text{He}^{2+}$	166	150.7	1.3546	1.291 (1.256, 1.372)	0.00 —
(2)†	2.5 MeV $^4\text{He}^{2+}$	166	150.7	1.3546	1.204 (1.094, 1.303)	0.51 (0.00, 5.96)
(2)†	1.8 MeV $^4\text{He}^{2+}$	200	154.6	1.6320	0.971 (0.890, 1.053)	0.00 —

Notes. The repair half-time was set to 2 h because the data sets contain only high-dose-rate radiation survival data. The 95% confidence intervals on estimated parameters are given in parentheses. DSB damage yields (Σ) were determined using the MCDS algorithm (16). The † indicates that LET, and subsequently \bar{z}_F , is potentially less than the reported value.

the statistics software R 1.7.1 and the L-BFGS-B optimization algorithm (37) implemented in FORTRAN 95.

To estimate confidence intervals, we use a paired bootstrap method (38) with random weights (39), which is often referred to as the Bayesian bootstrap (40). We use random weighting for “one experiment per dose/dose rate” designs, since standard bootstrap resampling (38) gives, with a large probability for small data sets, a degenerate answer when data with only one point for each dose are resampled.

RESULTS

LQ Radiosensitivity Parameters for Human Kidney T-1 Cells

Table 1 shows estimates of the LQ radiosensitivity parameters derived from the analysis of published cell survival data for human kidney T-1 cells. Because estimates of the α/β ratio are sometimes too high by factors as large as 6.2 when dose-rate effects are neglected in the analysis of high-dose-rate survival data (34), the protraction factor, G (Eq. 11), is computed with τ set to a representative value of 2 h. Radiosensitivity parameters are also derived for a wide range of other repair half-times (0.1–10 h) and the assumed value of the repair half-time has some impact on estimates of β for lower-LET radiations but no significant impact on the reported parameter estimates for higher-LET radiations (data not shown). As an example, point estimates of α and β vary from 0.711–0.725 Gy $^{-1}$ and 0.0090–0.0154 Gy $^{-2}$ for assumed repair half-times of 0.1 h and 10 h, respectively, for 25 MeV α particles (26 keV/ μm). For 1.8 MeV α particles (200 keV/ μm), estimates of α and β are independent of the assumed half-time for DSB repair. Table 1 shows that estimates of β tend to decrease as a function

of particle LET and approach zero for particles with LET ≥ 20 keV/ μm .

Contribution of Intrinsically Unrejoinable DSBs

The expressions relating LQ radiosensitivity parameters to the mechanisms of DSB induction and rejoining (Eqs. 9 and 10) can be used in conjunction with the estimates of α derived from the *in vitro* survival data to evaluate the contribution of potential mechanisms to cell killing through one-track mechanisms. Neglecting the potential effects of misrepaired and fixed DSBs ($\theta = 0$) and intratrack pairwise DSB interactions ($\kappa = 0$), Eq. (9) becomes

$$\alpha = (1 - f_R)\Sigma. \quad (13)$$

For an intrinsically unrejoinable DSB composed of $j = 7$ lesions, the values of α derived from the fit to the survival data are overestimated by a factor of 1.5 for the low-LET X rays and by a factor of ~ 30 for the high-LET 4 MeV α particles (Fig. 1). For $j = 10$ lesions, the derived values of α are underestimated by a factor of 22 for the low-LET X rays and overestimated by a factor of ~ 15 for the high-LET 4 MeV α particles. For $j = 15$ lesions, the value of α predicted by Eq. (13) is zero for the low-LET X rays and the derived value of α is overestimated by a factor of ~ 3 for the high-LET 4 MeV α particles. No other value of j (< 50) was found to be able to explain the trends in the data successfully. These observations suggest that all classes of DSB are potentially rejoinable. Alternatively, the number of lesions per cluster (j parameter in Eq. 1) may not provide the most appropriate scheme to subdivide

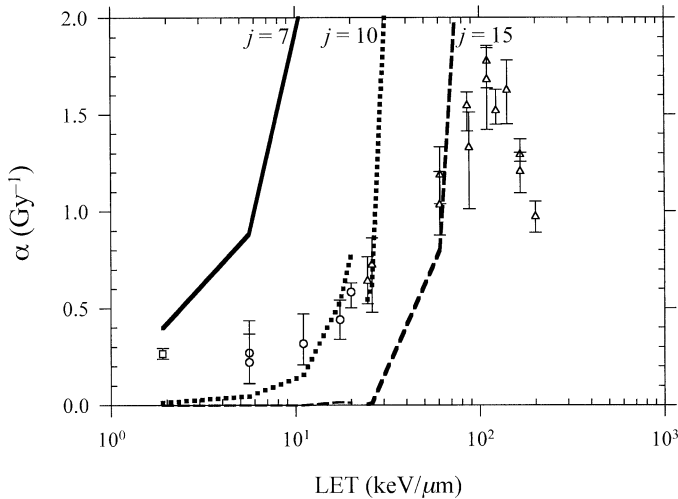


FIG. 1. Predictions of α assuming that only intrinsically unrejoinable DSBs contribute to one-track cell killing (Eq. 13). Open symbols are estimates of α derived from survival data for human kidney T-1 cells (1–4, 35). Squares, circles and triangles denote estimates derived from data for X rays, deuterons (${}^2\text{H}^+$) and α particles (${}^4\text{He}^{2+}$), respectively. Error bars are 95% confidence intervals on the α (Gy^{-1}) estimates. The solid, dotted and dashed lines show predictions of α assuming that 7, 10 or 15 lesions, respectively, render a DSB unrejoinable.

DSBs into rejoinable (*simple*) and unrejoinable (*complex*) DSBs.

Contribution of Misrepaired and Fixed DSBs

For the special case when all DSBs are considered potentially rejoinable ($f_R = 1$) and intratrack pairwise DSB interactions are neglected ($\kappa = 0$), Eq. (9) simplifies to

$$\alpha = \theta \bar{\Sigma}. \quad (14)$$

The solid line in Fig. 2A shows values of the α radiosenitivity parameter predicted using Eq. (14) with $\theta = 8.69 \times 10^{-3}$. The value of θ is determined from regression analysis of the α values derived from the cell survival data (up to $100 \text{ keV}/\mu\text{m}$). The discontinuity in the predicted values of α between 20 and 30 $\text{keV}/\mu\text{m}$ occurs because of differences in the initial DSB yield produced by deuterons and α particles. For particles with $\text{LET} \leq 26 \text{ keV}/\mu\text{m}$, the value of α predicted using Eq. (14) is consistently higher than the values derived directly from the survival data. For example, the α derived from survival data for X rays is overestimated by a factor of 1.6. For particles with $\text{LET} \geq 26 \text{ keV}/\mu\text{m}$, the predicted α values underestimate the values derived from the survival data, e.g., the α derived from survival data for 4 MeV α particles is underestimated by a factor of ~ 1.4 .

Contribution of Intratrack DSB Interactions

For the special case when all DSBs are potentially rejoinable ($f_R = 1$) and none of the DSBs are lethally misrepaired or fixed ($\theta = 0$), Eqs. (9) and (10) become

$$\alpha = \kappa \bar{z}_F \bar{\Sigma}^2 \quad \text{and} \quad (15)$$

$$\beta = (\kappa/2) \bar{\Sigma}^2, \quad (16)$$

where $\kappa = \gamma\eta/\lambda$. From Eq. (16), it follows that $\kappa = 2\beta/\bar{\Sigma}^2$. Values of \bar{z}_F estimated using Eq. (2) for an assumed cell nucleus $5 \mu\text{m}$ in diameter are shown in Table 1. For most ions, the concept of LET provides an accurate (within 10%) approximation for the energy deposited in a $5\text{-}\mu\text{m}$ target composed of water. A † in column 1 of Table 1 indicates that the deposition of energy within the target, and thus \bar{z}_F , may be more than 10% lower than the reported value. In particular, the formula for \bar{z}_F is known to be inaccurate for α particles with energy $< 4 \text{ MeV}$ (26).

Figure 2B shows values of the α radiosenitivity parameter predicted from Eq. (15) assuming that only intratrack DSB interactions contribute to one-track cell killing. As a first approximation, κ can be reasonably estimated using the nominal value for β derived from the regression analysis of the X-ray cell survival data, i.e., $\beta = 0.0265 \text{ Gy}^{-2}$. Predictions of α (solid line) are generated with Eq. (15) for a fixed fraction of initial DSBs that undergo lethal intratrack DSB interactions, i.e., $\kappa = 2(\beta/\bar{\Sigma}^2) = 2.11 \times 10^{-5}$. Predictions of α (dashed line) are also shown using Eq. (15) with $\kappa = 1.31 \times 10^{-4}$. This value of κ is determined from regression analysis of the α values derived from the cell survival data (up to $100 \text{ keV}/\mu\text{m}$). Both methods (fixed and variable κ) significantly underestimate the values of α derived from the survival data, especially for radiations with particle $\text{LET} \leq 26 \text{ keV}/\mu\text{m}$, with the exception of the predictions of α (dashed line) from the fit of Eq. (15) for particles with $\text{LET} \geq 61 \text{ keV}/\mu\text{m}$. α values predicted using Eq. (15) may be too high for particles with $\text{LET} > 100 \text{ keV}/\mu\text{m}$ because of uncertainties associated with estimates of the frequency-mean specific energy for high-LET particles. The results reported in these studies imply that the observed trends in α cannot be easily attributed to just intratrack pairwise DSB interactions.

Misrepaired and Fixed DSBs and Intratrack DSB Interactions

For the special case when all DSBs are potentially rejoinable ($f_R = 1$), Eq. (9) becomes

$$\alpha = \theta \bar{\Sigma} + \kappa \bar{z}_F \bar{\Sigma}^2. \quad (17)$$

Figure 3 shows values of the α radiosenitivity parameter (solid line) predicted using Eq. (17) with $\theta = 5.79 \times 10^{-3}$ and $\kappa = 5.59 \times 10^{-5}$ and values of the β radiosenitivity parameter (solid line) predicted using Eq. (16) with $\kappa = 5.59 \times 10^{-5}$. The values of θ and κ are determined from regression analysis of the α values derived from the cell survival data (up to $100 \text{ keV}/\mu\text{m}$). The value of κ determined from this fitting method is about 2.6 times larger than the value estimated with the β derived from the data for low-LET radiation (see the previous section). This is expected because, for high-LET radiation, the intratrack

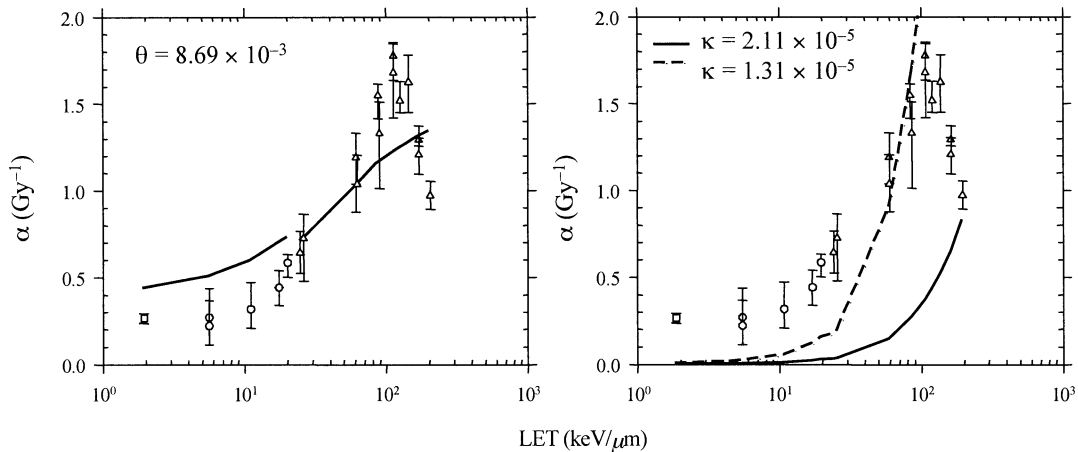


FIG. 2. Panel A: Predictions of α assuming only misrepaired and fixed DSBs contribute to one-track cell killing (solid line). Predictions are generated from a fit of Eq. (14) to the α estimates derived from survival data up to 100 keV/μm. Panel B: Predictions of α assuming only intratrack DSB interactions contribute to one-track cell killing. The solid line shows predictions of α generated using Eq. (15) for a fixed value of $\kappa = 2(\beta/\Sigma^2)$. The dashed line shows predictions of α generated from a fit of Eq. (15) to the α estimates derived from survival data up to 100 keV/μm. Open symbols are estimates of α derived from survival data for human kidney T-1 cells (1-4, 35). Squares, circles and triangles denote estimates derived from data for X rays, deuterons (${}^2\text{H}^+$) and α particles (${}^4\text{He}^{2+}$), respectively. Error bars are 95% confidence intervals on the α (Gy⁻¹) estimates.

pairwise interaction rate is expected to be larger than the intertrack pairwise interaction rate due to proximity effects (41). The dashed line shows the contribution to one-track cell killing from misrepaired and fixed DSBs ($\kappa = 0$), while the dotted line shows the contribution of intratrack DSB interactions ($\theta = 0$). Intratrack DSB interactions are negligible for low-LET radiations because the probability that a single track creates more than one DSB is very low (~0.8 DSBs per track for X rays). For 200 and 250 kVp X rays

(~1.9 keV/μm), a maximum of 99% of the one-track killing is due to misrepaired and fixed DSBs and 1% is due to intratrack DSB interactions. As particle LET increases, the probability that a single track of radiation creates more than one DSB increases (~125 DSBs per track for 4 MeV α particles), and subsequently, the importance of intratrack pairwise DSB interactions increases. However, misrepaired and fixed DSBs still contribute significantly to cell killing for high-LET radiations through one-track mechanisms. For

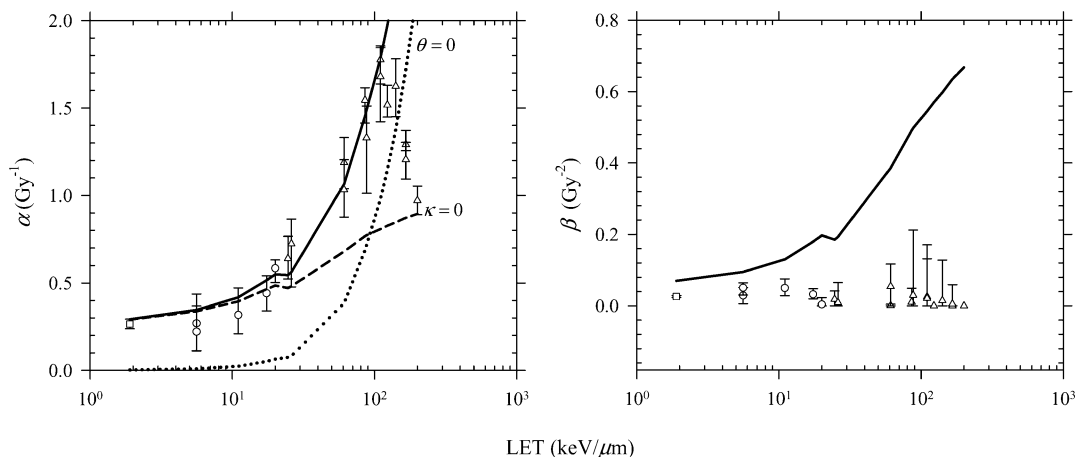


FIG. 3. Predictions of α (panel A) and β (panel B) assuming misrepaired and fixed DSBs and intratrack DSB interactions contribute to one-track cell killing (Eq. 17) and intertrack DSB interactions contribute to two-track cell killing (Eq. 16). Open symbols are estimates of α and β derived from survival data for human kidney T-1 cells (1-4, 35). Squares, circles and triangles denote estimates derived from data for X rays, deuterons (${}^2\text{H}^+$) and α particles (${}^4\text{He}^{2+}$), respectively. Error bars are 95% confidence intervals on α (Gy⁻¹) and β (Gy⁻²) estimates. Predictions of α (solid line) are generated from a two-parameter fit of Eq. (17) to the estimates of α derived from survival data up to 100 keV/μm ($\theta = 5.79 \times 10^{-3}$, $\kappa = 5.59 \times 10^{-5}$). Dashed and dotted lines represent the components of α due to misrepaired and fixed DSBs ($\kappa = 0$) and intratrack DSB interactions ($\theta = 0$), respectively. Predictions of β (solid line) are generated from Eq. (16) for $\kappa = 5.59 \times 10^{-5}$.

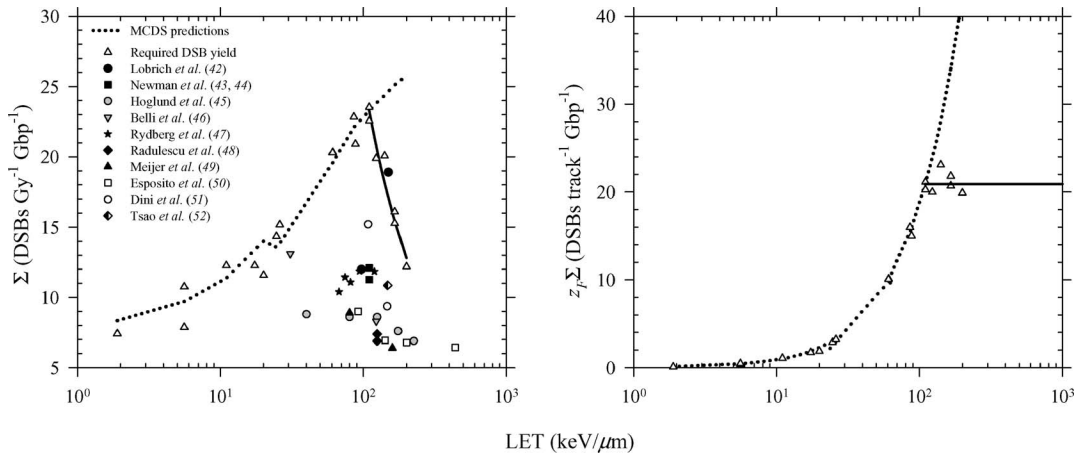


FIG. 4. Predicted and experimental DSB yields. Open triangles show the values of Σ (panel A) and $\bar{z}_F \Sigma$ (panel B) necessary to predict (Eq. 17) the estimates of α derived from a fit to the cell survival data. Dotted lines show the Monte Carlo damage simulation (MCDS) predictions of Σ (panel A) and $\bar{z}_F \Sigma$ (panel B). Experimental DSB yields reported in the literature are also shown. The solid line in panel A indicates the DSB yield if $\bar{z}_F \Sigma$ is assumed to be constant (125 DSBs cell⁻¹) above 110 keV/ μm . The solid line in panel B indicates the assumed constant $\bar{z}_F \Sigma$ (125 DSBs cell⁻¹) above 110 keV/ μm .

5.1 MeV α particles (~ 88 keV/ μm), a maximum of 52% of the one-track killing is due to misrepaired and fixed DSBs and 48% is due to intratrack DSB interactions.

Equation (17) fails to capture the downward trend in α for particles with LET > 110 keV/ μm . Potential explanations for the decrease in α above 110 keV/ μm include a decrease in the expected number of DSBs Gy⁻¹ cell⁻¹ (Σ parameter) or a decrease in the fraction of DSBs that undergo lethal intratrack pairwise interaction, $\kappa = [\eta/\lambda][\gamma - \theta]$. Figure 4 shows the necessary values of Σ (panel A) and $\bar{z}_F \Sigma$ (panel B) required to predict the trends in α as a function of LET using Eq. (17). Dotted lines represent the MCDS predictions of Σ (panel A) and $\bar{z}_F \Sigma$ (panel B). For comparison to the MCDS-predicted damage yields, which are similar to the absolute and relative DSB yields predicted by detailed track structure simulations (16), Fig. 4 also shows DSB yields obtained using DNA fragmentation analysis (42–52). The DSB yields predicted by the MCDS algorithm need to be lower by a factor of 1.2–2.1 for the low-energy (high-LET) α particles to predict the trends in α above 110 keV/ μm .

The solid line in Fig. 4 shows the predicted trend in the DSB yield obtained when it is assumed that $\bar{z}_F \Sigma$ is constant above 110 keV/ μm . The potential justification for this assumption is that the probability a DSB occurs in a DNA segment after a particle crossing should approach unity as LET increases [see Eq. (4) and related discussion]. If this assumption is correct, the downward trend in the estimates of α above 110 keV/ μm can be predicted accurately if $\bar{z}_F \Sigma$ approaches the asymptotic value of 125 DSBs track⁻¹ cell⁻¹ (Fig. 4B, solid line). A constant value for $\bar{z}_F \Sigma$ above 110 keV/ μm results in decreasing values of Σ (Fig. 4A, solid line) because \bar{z}_F continues to increase with increasing LET. Although uncertainties associated with \bar{z}_F , especially above

110 keV/ μm , may have some impact, the trends in α with particle LET cannot be explained easily without also assuming that Σ is lower than the value predicted with the MCDS program or that the rates (e.g., the balance between repair and misrepair) or accuracy of DSB rejoining change substantially for particles with LET greater than about 100 keV/ μm . Figure 5 shows the necessary decrease in the fraction of DSBs that undergo lethal intratrack pairwise interaction, κ , to predict the trends in α as a function of particle LET. Decreasing values of κ suggest that either the ratio of the second-order, η , and first-order, λ , repair rates decreases as particle LET increases or the fraction, γ , of lethal exchange-type aberrations decreases as particle LET increases (see Eq. 17).

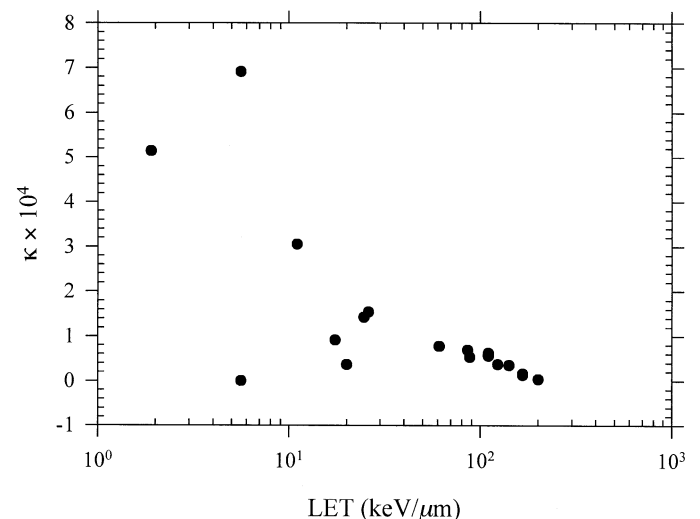


FIG. 5. Values of κ necessary to predict (Eq. 17) the estimates of α derived from a fit to the cell survival data.

DISCUSSION

In the new RMF model presented in this article, reproductive cell death is attributed to DSB induction and processing, i.e., to the conversion of DSBs into lethal exchanges through intra- and intertrack binary misrepair or through the formation of unrepairable or misrepaired DSBs. The exact relationships between the induction of lethal forms of damage and specific cell death modes (e.g., necrosis or apoptosis) are implicitly included in the RMF model through parameters that relate the yield of misrepaired or fixed damage to the probability that a cell remains reproductively viable. The near one-to-one correspondence between asymmetric exchanges and the logarithm of the surviving fraction observed in AG1522 normal human fibroblasts (9) is an elegant demonstration that the conversion of DSBs into lethal exchanges is an especially important mechanism of reproductive death in at least one human cell line. Although DNA damage is an initiating event for the induction of apoptosis, radiation damage to cellular membranes can also initiate apoptosis [reviewed in ref. (53)]. Clustered damage other than the DSBs may also contribute to cell killing. Because estimates of α and β (Table 1) include all cell death modes and mechanisms, estimates of the θ and κ parameters derived from Eqs. (9) and (10) are most likely too high. However, trends in α with particle LET can be predicted accurately up to about 100 keV/ μm with the same values for θ and κ (solid line in Fig. 3). This observation is consistent with the hypothesis that the effects of LET on cell killing may arise through processes linked to the induction and processing of DSBs, especially intra- and intertrack binary misrepair, as postulated in the RMF model.

The expressions relating LQ radiosensitivity parameters to DSB induction, rejoining and fixation (Eqs. 9 and 10) suggest that the β cell killing mechanism arises because pairs of DSBs formed by different tracks are sometimes misrejoined to form lethal exchanges, such as dicentric and centric rings. Because chromosome aberration studies [(41, 54–57) and references therein] provide direct evidence that exchanges are formed at substantial levels by high-LET radiations, we hypothesize that β should be greater than zero even for high-LET radiations. That is, break ends associated with pairs of DSBs formed by high-LET radiations are sometimes misrejoined to form exchanges. Panel B of Fig. 3 shows model predictions of the β radiosensitivity parameter (solid line) generated from Eq. (16) for $\kappa = 5.59 \times 10^{-5}$. Discrepancies between model-predicted parameter values and those derived from experimental data are as large as two orders of magnitude. A plausible explanation for the tendency of two-parameter fits to give decreasing values of β as particle LET increases is that the doses used in the *in vitro* experiments are not large enough for the βGD^2 term to have a substantial impact on cell killing. The observed downward trend in β as a function of particle LET is most likely an artifact of the measured data and the fitting procedure rather than a reflection of the true biophysical

mechanisms responsible for cell killing. As an alternative to the intertrack pairwise DSB interaction mechanism, others (58) have suggested that exchanges may be formed through the interaction of damaged and undamaged chromatin regions. This hypothesis implies that β may be zero for some types of radiation.

Although stochastic models (59–61) provide a more accurate representation of the binary misrepair process, estimates of the surviving fraction determined using stochastic and deterministic binary misrepair models are quite similar (60, 61). Also, the computational requirements of a fully stochastic model are sometimes prohibitive for practical applications. Several groups (62–66) have developed models to investigate the increased RBE of high-LET radiation. Track structure models (62, 63) suggest that RBE depends on the structure of the radiation track and the capacity for biological repair. Moiseenko *et al.* (64) have analyzed experimental data for exchange-type chromosome aberrations (dicentrics) in human lymphocytes. They concluded that a pathway for the production of exchanges in proportion to dose must exist and that it does not involve the pairwise interaction of DSBs. As shown in the RMF model, intratrack binary misrepair does give rise to a term for the production of exchanges that is proportional to dose. The term proportional to dose arises because terms related to intra- and intertrack binary misrepair are derived using a compound binomial model for DSB induction rather than a Poisson distribution.

Intratrack binary misrepair gives rise to a term that is dependent on the expected number of DSBs formed per track, i.e., $\bar{z}_F \Sigma$. For a cell nucleus with an approximate diameter of 5 μm , the frequency-mean specific energy for low-LET radiation ($\text{LET} \leq 1 \text{ keV}/\mu\text{m}$) is less than or equal to approximately 10 mGy, and the expected number of DSBs formed per cell by a low-LET radiation track is ~ 0.4 . The probability that a single low-LET radiation track will create two or more DSBs in the same cell, assuming Poisson statistics for damage induction per track, is less than 7%. For comparison, the probability two or more DSBs will be created by the passage of a 2 MeV α particle ($\text{LET} = 162.5 \text{ keV}/\mu\text{m}$, $\Sigma = 150.2 \text{ DSBs Gy}^{-1} \text{ cell}^{-1}$) through the nucleus is close to unity. This observation suggests that intratrack binary misrepair is much more important for high-LET radiation than for low-LET radiation. Indeed, the reported analyses suggest that, for low-LET radiation, the contribution of intratrack binary misrepair to cell killing is negligible ($< 0.7\%$).

The observation that intratrack binary misrepair is unlikely to be responsible for the majority of the lethal one-track (α) damage suggests that unrejoinable, misrepaired or fixed damage may contribute substantially to cell killing, especially for low-LET radiations. The analysis in the section on the contribution of intrinsically unrejoinable DSBs suggests that no DSBs, even very complex DSBs composed of many lesions, are *intrinsically* unrejoinable. Rather, extrinsic processes such as damage fixation or biochemical repair must convert a subset of the initial damage into unrejoinable forms of damage

(e.g., acentric fragments) or into small-scale mutations. Damage fixation and biochemical repair are kinetic processes that convert some initial form of radiation damage into an irreversible and lethal type of damage, whereas intrinsically unrejoinable damage has no chance of ever undergoing biochemical repair and is lethal at the instant in time it is created. However, it is possible that the number of lesions per cluster [j parameter in Eq. (1)] may not be an appropriate scheme to subdivide DSBs into rejoinable and unrejoinable DSBs. Alternatively, the poor correlation between the induction of complex, intrinsically unrejoinable DSBs and trends in one-track lethal damage may be due to limitations of the Monte Carlo model used to simulate damage induction (e.g., the nucleotide-level maps provided by the MCDS program may not be completely accurate).

The two major pathways available to rejoin DSBs are homologous recombination (HR) and non-homologous end joining (NHEJ). The NHEJ pathway is the primary repair mechanism responsible for DSB rejoining in mammalian cells, especially in G_0 and G_1 -phase cells, although HR also contributes to DSB rejoining (67–69). Although NHEJ can in general be an error-free or error-prone repair process, rejoining of even correct break ends associated with a single DSB most likely results in the formation of small-scale insertions or deletions rather than correct repair (restoration of the original base sequence). Radiation, even low-LET radiation, frequently creates clusters with multiple DNA lesions within one or two turns of the DNA (24), which implies that sequence information is usually lost in a section of DNA containing a radiation-induced cluster. If small-scale mutations formed through DSB misrepair are sometimes lethal, then small-scale mutations formed through the misrepair of non-DSB clusters may also be lethal.

The MCDS model (16) predicts that 1 MeV (low-LET) electrons create about 190 SSBs $Gy^{-1} Gbp^{-1}$ and 430 sites of base damage $Gy^{-1} Gbp^{-1}$. Monte Carlo simulations (70, 71) of the long-patch base excision repair (BER) of non-DSB clusters suggest that about 2% of the base damage and 4% of the SSBs are misrepaired. The Monte Carlo BER model also predicts that about 3% of the SSBs will be converted to DSBs through unsuccessful excision repair events. The expected number of small-scale mutations formed through the misrepair of non-DSB clusters is the product of the damage yield and the probability the damage is misrepaired. For 1 MeV electrons, the attempted repair of non-DSB clusters has the potential to create about 64 small-scale mutations $Gy^{-1} Gbp^{-1}$ and an additional 5.7 DSBs $Gy^{-1} Gbp^{-1}$ through unsuccessful excision repair of SSBs. For comparison, the MCDS program predicts that 1 MeV electrons create about 8.3 DSBs $Gy^{-1} Gbp^{-1}$ (16), which corresponds to a maximum of 8.3 unrepairable or small-scale mutations $Gy^{-1} Gbp^{-1}$. This comparison of damage and mutation yields suggests that, for low-LET radiation, non-DSB clusters may be a more important source of one-track lethal damage than the DSBs formed directly by ionizing radiation.

Figure 4 (solid lines and open triangles) suggests that a decrease in the expected number of DSBs is a potential explanation for the downward trend in α beyond 110 $keV/\mu m$. The measured DSB yields (42–52) shown in Fig. 4 do not exhibit a clear upward or downward trend with LET. Another potential issue is that the DSB yields predicted by the MCDS algorithm are substantially larger than experimental estimates reported in the literature. For example, Newman *et al.* (44) report that 2.5 MeV α particles induce approximately 12 DSBs $Gy^{-1} Gbp^{-1}$ in the DNA of V79 cells, and Rydberg *et al.* (47) report that 3–7 MeV α particles induce 10.4–11.8 DSBs $Gy^{-1} Gbp^{-1}$ in the DNA of GM38 human fibroblast cells. In contrast, the MCDS algorithm predicts yields of 20–24 DSBs $Gy^{-1} Gbp^{-1}$ for α particles in the same energy range. These differences between the MCDS-predicted and experimental DSB yields are not unexpected since parameters used in the MCDS algorithm have been chosen to reproduce track-structure simulations that give only approximate agreement with the experimental DSB yields (22, 23, 47). The low DSB yields reported in experimental studies may be related to limitations of the widely used pulsed-field gel electrophoresis (PFGE) assay; i.e., small fragments of the DNA may be lost during the experiment, which results in lower estimates of the DSB yield (23, 47). Regardless, the predicted trends in α and β with particle LET are not overly sensitive to the absolute DSB yield because the formulas for α and β involve the product of θ and Σ or κ and Σ^2 . Hence a possible systematic overestimation of Σ by the MCDS algorithm will be offset by systematically lower values for θ and κ .

The rates (e.g., the balance between repair and misrepair) or accuracy of DSB rejoining may change substantially for particles with LET greater than 110 $keV/\mu m$. Sachs and Brenner (41) suggest that the ratio of the exchange-rate and restitution-rate constants (η/λ) increases as a function of particle LET due to the increased production of “severe” DSBs that are long-lived and prone to form exchanges. Brenner (72) and Sachs *et al.* (73) also suggest that proximity effects, i.e., a decrease in the spatial separation between DSBs formed by high-LET radiation, lead to an increased probability of binary misrepair and therefore to an increase in the ratio of η/λ . However, proximity effects increase the ratio of intra-arm to interarm exchanges (73), i.e., the ratio of exchanges on the same arm of the same chromosome to exchanges formed on opposing arms of the same chromosome. Sachs *et al.* (74) report that intra-arm exchanges (acentric rings or paracentric inversions) relative to interarm exchanges (centric rings or pericentric inversions) are increased up to tenfold by proximity effects. An increase in the ratio η/λ is expected to result in an increase in the fraction of DSBs that undergo lethal intratrack pairwise interactions, κ , while an increase in the formation of intra-arm exchanges by high-LET radiation is expected to result in a decrease in the fraction of lethal exchanges, γ , and subsequently a decrease in κ (see Fig. 5).

CONCLUSIONS

To the best of our knowledge, the reported studies are the first to directly use estimates of damage yields from Monte Carlo simulations to examine the effects of intrinsically unrejoinable DSBs, extrinsic damage fixation, and intratrack DSB interactions. The proposed approach provides many useful opportunities to probe and quantify the biological mechanisms presumably underlying the cell killing effects of low- and high-LET radiations. The reported analyses of *in vitro* survival data for human kidney T-1 cells suggest that the trends in the radiosensitivity parameter α are well predicted up to ~ 100 keV/ μm by biologically motivated expressions that explicitly account for the formation of lethal damage as a result of misrepaired and fixed DSBs and intratrack DSB interactions. The reported studies suggest that all classes of DSBs may be potentially rejoinable. Even very complex DSBs composed of 10 or more lesions may be potentially rejoinable. Alternatively, the number of lesions forming the DSB may not be a useful way to the classify DSBs into repairable and unrepairable forms of damage. The reported studies suggest that intratrack DSB interactions are negligible for low-LET radiations because these radiations are unlikely to produce more than one DSB per track. For 200 and 250 kVp X rays (~ 1.9 keV/ μm), a maximum of 99% of the one-track killing is due to misrepaired and fixed DSBs and 1% is due to intratrack DSB interactions. The importance of intratrack pairwise DSB interactions increases with increasing LET. However, misrepaired and fixed DSBs still contribute to cell killing through one-track mechanisms. For 5.1 MeV α particles (~ 88 keV/ μm), a maximum of 52% of the one-track killing is due to misrepaired and fixed DSBs and 48% is due to intratrack DSB interactions. The increased RBE of high-LET radiations is attributed to the increased numbers of DSBs cell⁻¹, and the local complexity of DSBs has a small or negligible impact on the ultimate lethal damage yield. The contribution of lethal exchanges formed through intratrack mechanisms increases substantially with particle LET. The reported studies provide new insight into the underlying mechanisms of cell killing by low- and high-LET particles.

The advancement of our understanding of the mechanisms underlying the radiation response of tumor and normal tissues will ultimately result in the refinement of models to predict the survival of cells exposed to high-LET radiation. Beams of energetic protons and more massive ions, such as carbon, have become increasingly more common in cancer therapy due to their potential to improve the probability of tumor control (75, 76). Since the probability models for tumor control and normal-tissue complications are intimately linked to the induction and processing of DNA damage, our ability to understand the increased efficacy of these high-LET radiations relies on basic understanding of their biophysical mechanisms of action. The incorporation of information from Monte Carlo simulations

into the biologically motivated expressions to predict changes in intrinsic radiation sensitivity parameters has the potential to improve the predictive power of models of radiation-induced cell killing without the need to introduce an inordinate number of purely adjustable biological parameters into the modeling process.

Received: March 28, 2007; accepted: December 19, 2007

REFERENCES

1. G. W. Barendsen, T. L. Beusker, A. J. Vergroesen and L. Budke, Effects of different radiations on human cells in tissue culture. II. Biological experiments. *Radiat. Res.* **13**, 841–849 (1960).
2. G. W. Barendsen, Impairment of the proliferative capacity of human cells in culture by alpha-particles with differing linear-energy transfer. *Int. J. Radiat. Biol. Relat. Stud. Phys. Chem. Med.* **8**, 453–466 (1964).
3. G. W. Barendsen and H. M. D. Walter, Effects of different ionizing radiations on human cells in tissue culture. *Radiat. Res.* **21**, 314–329 (1964).
4. G. W. Barendsen, C. J. Koot, G. R. Van Kersen, D. K. Bewley, S. B. Field and C. J. Parnell, The effect of oxygen on impairment of the proliferative capacity of human cells in culture by ionizing radiations of different LET. *Int. J. Radiat. Biol. Relat. Stud. Phys. Chem. Med.* **10**, 317–327 (1966).
5. Y. Furusawa, K. Fukutsu, M. Aoki, H. Itsukaichi, K. Eguchi-Kasai, H. Ohara, F. Yatagai, T. Kanai and K. Ando, Inactivation of aerobic and hypoxic cells from three different cell lines by accelerated ³He-, ¹²C- and ²⁰Ne-ion beams. *Radiat. Res.* **154**, 485–496 (2000).
6. C. Tsuruoka, M. Suzuki, T. Kanai and K. Fujitaka, LET and ion species dependence for cell killing in normal human skin fibroblasts. *Radiat. Res.* **163**, 494–500 (2005).
7. W. K. Weyrather, S. Ritter, M. Scholz and G. Kraft, RBE for carbon track-segment irradiation in cell lines of differing repair capacity. *Int. J. Radiat. Biol.* **75**, 1357–1364 (1999).
8. R. Okayasu, M. Okada, A. Okabe, M. Noguchi, K. Takakura and S. Takahashi, Repair of DNA damage induced by accelerated heavy ions in mammalian cells proficient and deficient in the non-homologous end-joining pathway. *Radiat. Res.* **165**, 59–67 (2006).
9. M. N. Cornforth and J. S. Bedford, A quantitative comparison of potentially lethal damage repair and the rejoining of interphase chromosome breaks in low passage normal human fibroblasts. *Radiat. Res.* **111**, 385–405 (1987).
10. J. S. Bedford, Sublethal damage, potentially lethal damage, and chromosomal aberrations in mammalian cells exposed to ionizing radiations. *Int. J. Radiat. Oncol. Biol. Phys.* **21**, 1457–1469 (1991).
11. J. T. Lett, A. B. Cox and D. S. Bergtold, Cellular and tissue responses to heavy ions: basic considerations. *Radiat. Environ. Biophys.* **25**, 1–12 (1986).
12. D. Frankenberg, H. J. Brede, U. J. Schrewe, C. Steinmetz, M. Frankenberg-Schwager, G. Kasten and E. Pralle, Induction of DNA double-strand breaks by ¹H and ⁴He ions in primary human skin fibroblasts in the LET range of 8 to 124 keV/ μm . *Radiat. Res.* **151**, 540–549 (1999).
13. G. Taucher-Scholz and G. Kraft, Influence of radiation quality on the yield of DNA strand breaks in SV40 DNA irradiated in solution. *Radiat. Res.* **151**, 595–604 (1999).
14. J. F. Ward, DNA damage produced by ionizing radiation in mammalian cells: identities, mechanisms of formation, and reparability. *Prog. Nucleic Acid Res. Mol. Biol.* **35**, 95–125 (1988).
15. D. T. Goodhead, Initial events in the cellular effects of ionizing radiations: clustered damage in DNA. *Int. J. Radiat. Biol.* **65**, 7–17 (1994).
16. V. A. Semenenko and R. D. Stewart, Fast Monte Carlo simulation of DNA damage formed by electrons and light ions. *Phys. Med. Biol.* **51**, 1693–1706 (2006).

17. C. A. Tobias, The repair-misrepair model in radiobiology: comparison to other models. *Radiat. Res. Suppl.* **8**, S77–S95 (1985).
18. S. B. Curtis, Lethal and potentially lethal lesions induced by radiation—a unified repair model. *Radiat. Res.* **106**, 252–270 (1986).
19. L. Hlatky, R. K. Sachs, M. Vazquez and M. N. Cornforth, Radiation-induced chromosome aberrations: insights gained from biophysical modeling. *BioEssays* **24**, 714–723 (2002).
20. R. K. Sachs, P. Hahnfeldt and D. J. Brenner, The link between low-LET dose-response and the underlying kinetic of damage production/repair/misrepair. *Int. J. Radiat. Biol.* **72**, 351–374 (1997).
21. H. Nikjoo, P. O'Neill, W. E. Wilson and D. T. Goodhead, Computational approach for determining the spectrum of DNA damage induced by ionizing radiation. *Radiat. Res.* **156**, 577–583 (2001).
22. W. Friedland, P. Jacob, P. Bernhardt, H. G. Paretzke and M. Dingfelder, Simulation of DNA damage after proton irradiation. *Radiat. Res.* **159**, 401–410 (2003).
23. W. Friedland, M. Dingfelder, P. Jacob and H. G. Paretzke, Calculated DNA double-strand break and fragmentation yields after irradiation with He ions. *Radiat. Phys. Chem.* **72**, 279–286 (2005).
24. V. A. Semenenko and R. D. Stewart, A fast Monte Carlo algorithm to simulate the spectrum of DNA damages formed by ionizing radiation. *Radiat. Res.* **161**, 451–457 (2004).
25. ICRU, *Microdosimetry*. Report 36, International Commission of Radiation Units and Measurements, Bethesda, MD, 1983.
26. A. M. Kellerer and D. Chmelevsky, Criteria for the applicability of LET. *Radiat. Res.* **63**, 226–234 (1975).
27. E. Gudowska-Nowak, S. Ritter, G. Taucher-Scholz and G. Kraft, Compound Poisson processes and clustered damage of radiation induced DNA double strand breaks. *Acta Phys. Polon. B* **31**, 1109–1124 (2000).
28. T. Straume and J. N. Lucas, A comparison of the yields of translocations and dicentric chromosomes measured using fluorescence *in situ* hybridization. *Int. J. Radiat. Biol.* **64**, 185–187 (1993).
29. A. M. Kellerer and H. H. Rossi, A generalized formulation of dual radiation action. *Radiat. Res.* **75**, 471–488 (1978).
30. R. G. Dale, The application of the linear-quadratic dose-effect equation to fractionated and protracted radiotherapy. *Br. J. Radiol.* **58**, 515–528 (1985).
31. H. D. Thames, An 'incomplete-repair' model for survival after fractionated and continuous irradiations. *Int. J. Radiat. Biol. Relat. Stud. Phys. Chem. Med.* **47**, 319–339 (1985).
32. D. J. Brenner, L. R. Hlatky, P. J. Hahnfeldt, Y. Huang and R. K. Sachs, The linear-quadratic model and most other common radiobiological models result in similar predictions of time-dose relationships. *Radiat. Res.* **150**, 83–91 (1998).
33. M. Guerrero, R. D. Stewart, J. Z. Wang and X. A. Li, Equivalence of the linear-quadratic and two-lesion kinetic models. *Phys. Med. Biol.* **47**, 3197–3209 (2002).
34. D. J. Carlson, R. D. Stewart, X. A. Li, K. Jennings, J. Z. Wang and M. Guerrero, Comparison of *in vitro* and *in vivo* α/β ratios for prostate cancer. *Phys. Med. Biol.* **49**, 4477–4491 (2004).
35. G. W. Barendsen, H. M. Walter, J. F. Fowler and D. K. Bewley, Effects of different ionizing radiations on human cells in tissue culture. III. Experiments with cyclotron-accelerated alpha-particles and deuterons. *Radiat. Res.* **18**, 106–119 (1963).
36. D. J. Carlson, R. D. Stewart and V. A. Semenenko, Effects of oxygen on intrinsic radiation sensitivity: A test of the relationship between aerobic and hypoxic linear-quadratic (LQ) model parameters. *Med. Phys.* **33**, 3105–3115 (2006).
37. R. H. Byrd, P. Lu and J. Nocedal, A limited memory algorithm for bound constrained optimization. *SIAM J. Sci. Stat. Comput.* **16**, 1190–1208 (1995).
38. B. Efron, Bootstrap methods: Another look at the jackknife. *Ann. Stat.* **7**, 1–26 (1979).
39. Z. Zheng, Random weighting methods. *Acta Math. Appl. Sinica* **10**, 247–253 (1987).
40. D. B. Rubin, The Bayesian bootstrap. *Ann. Stat.* **9**, 130–134 (1981).
41. R. K. Sachs and D. J. Brenner, Effect of LET on chromosomal aberration yields. I. Do long-lived, exchange-prone double strand breaks play a role? *Int. J. Radiat. Biol.* **64**, 677–688 (1993).
42. M. Löbrich, P. K. Cooper and B. Rydberg, Non-random distribution of DNA double-strand breaks induced by particle irradiation. *Int. J. Radiat. Biol.* **70**, 493–503 (1996).
43. H. C. Newman, K. M. Prise, M. Folkard and B. D. Michael, DNA double-strand break distributions in X-ray and alpha-particle irradiated V79 cells: evidence for non-random breakage. *Int. J. Radiat. Biol.* **71**, 347–363 (1997).
44. H. C. Newman, K. M. Prise and B. D. Michael, The role of higher-order chromatin structure in the yield and distribution of DNA double-strand breaks in cells irradiated with X-rays or alpha-particles. *Int. J. Radiat. Biol.* **76**, 1085–1093 (2000).
45. E. Höglund, E. Blomquist, J. Carlsson and B. Stenerlöw, DNA damage induced by radiation of different linear energy transfer: initial fragmentation. *Int. J. Radiat. Biol.* **76**, 539–547 (2000).
46. M. Belli, R. Cherubini, M. Dalla Vecchia, V. Dini, G. Esposito, G. Moschini, O. Sapora, G. Simone and M. A. Tabocchini, DNA fragmentation in V79 cells irradiated with light ions as measured by pulsed-field gel electrophoresis. I. Experimental results. *Int. J. Radiat. Biol.* **78**, 475–482 (2002).
47. B. Rydberg, L. Heilbronn, W. R. Holley, M. Löbrich, C. Zeitlin, A. Chatterjee and P. K. Cooper, Spatial distribution and yield of DNA double-strand breaks induced by 3–7 MeV helium ions in human fibroblasts. *Radiat. Res.* **158**, 32–42 (2002).
48. I. Radulescu, K. Elmroth and B. Stenerlöw, Chromatin organization contributes to non-randomly distributed double-strand breaks after exposure to high-LET radiation. *Radiat. Res.* **161**, 1–8 (2004).
49. A. E. Meijer, A. R. Jernberg, T. Heiden, B. Stenerlöw, L. M. Persson, N. Tilly, B. K. Lind and M. R. Edgren, Dose and time dependent apoptotic response in a human melanoma cell line exposed to accelerated boron ions at four different LET. *Int. J. Radiat. Biol.* **81**, 261–272 (2005).
50. G. Esposito, F. Antonelli, M. Belli, A. Campa, V. Dini, Y. Furusawa, G. Simone, E. Sorrentino and M. A. Tabocchini, DNA DSB induced by iron ions in human fibroblasts: LET dependence and shielding efficiency. *Adv. Space Res.* **35**, 243–248 (2005).
51. V. Dini, F. Antonelli, M. Belli, A. Campa, G. Esposito, G. Simone, E. Sorrentino and M. A. Tabocchini, Influence of PMMA shielding on DNA fragmentation induced in human fibroblasts by iron and titanium ions. *Radiat. Res.* **164**, 577–581 (2005).
52. D. Tsao, P. Kalogerinis, I. Tabrizi, M. Dingfelder, R. D. Stewart and A. G. Georgakilas, Induction and processing of oxidative clustered DNA lesions in ^{56}Fe -ion-irradiated human monocytes. *Radiat. Res.* **168**, 87–97 (2007).
53. I. R. Radford, Initiation of ionizing radiation-induced apoptosis: DNA damage-mediated or does ceramide have a role? *Int. J. Radiat. Biol.* **75**, 521–528 (1999).
54. J. J. Boei, S. Vermeulen, L. H. Mullenders and A. T. Natarajan, Impact of radiation quality on the spectrum of induced chromosome exchange aberrations. *Int. J. Radiat. Biol.* **77**, 847–857 (2001).
55. J. L. Schwartz and A. W. Hsie, Genetic and cytogenetic markers of exposure to high-linear energy transfer radiation. *Radiat. Res.* **148** (Suppl.), S87–S92 (1997).
56. M. S. Sasaki, T. Takatsuji and Y. Ejima, The F value cannot be ruled out as a chromosomal fingerprint of radiation quality. *Radiat. Res.* **150**, 253–258 (1998).
57. B. Rydberg, B. Cooper, P. K. Cooper, W. R. Holley and A. Chatterjee, Dose-dependent misjoining of radiation-induced DNA double-strand breaks in human fibroblasts: Experimental and theoretical study for high- and low-LET radiation. *Radiat. Res.* **163**, 526–534 (2005).
58. R. Greinert, C. Thieke, E. Detzler, O. Boguhn, D. Frankenberg and D. Harder, Chromosome aberrations induced in human lymphocytes by 3.45 MeV alpha particles analyzed by premature chromosome condensation. *Radiat. Res.* **152**, 412–420 (1999).
59. N. Albright, A Markov formulation of the repair-misrepair model of cell survival. *Radiat. Res.* **118**, 1–20 (1989).

60. R. K. Sachs, L. Hlatky, P. Hahnfeldt and P. L. Chen, Incorporating dose-rate effects in Markov radiation cell survival models. *Radiat. Res.* **124**, 216–226 (1990).
61. R. K. Sachs and L. R. Hlatky, Dose-rate dependent stochastic effects in radiation cell-survival models. *Radiat. Environ. Biophys.* **29**, 169–184 (1990).
62. M. Scholz and G. Kraft, A parameter free track structure model for heavy ion action cross sections. In *Biophysical Modelling of Radiation Effects* (K. H. Chadwick, G. Moschini and M. N. Varma, Eds.), pp. 185–192. Adam Hilger, New York, 1992.
63. R. Katz, F. A. Cucinotta, J. W. Wilson, J. L. Shinn and D. M. Ngo, A model of cell damage in space flight. In *Biological Effects and Physics of Solar and Galactic Cosmic Radiation, Part A* (C. E. Swenberg, G. Horneck and E. G. Stassinopoulos, Eds.), pp. 235–268. Plenum Press, New York, 1993.
64. V. V. Moiseenko, A. A. Edwards, H. Nikjoo and W. V. Prestwich, The influence of track structure on the understanding of relative biological effectiveness for induction of chromosomal exchanges in human lymphocytes. *Radiat. Res.* **147**, 208–214 (1997).
65. R. B. Hawkins, A microdosimetric-kinetic model for the effect of non-Poisson distribution of lethal lesions on the variation of RBE with LET. *Radiat. Res.* **160**, 61–69 (2003).
66. P. Kunderát, Detailed analysis of the cell-inactivation mechanism by accelerated protons and light ions. *Phys. Med. Biol.* **51**, 1185–1199 (2006).
67. R. D. Johnson and M. Jasin, Double-strand-break-induced homologous recombination in mammalian cells. *Biochem. Soc. Trans.* **29**, 196–201 (2001).
68. S. P. Jackson, Sensing and repairing DNA double-strand breaks. *Carcinogenesis* **23**, 687–696 (2002).
69. P. A. Jeggo, The fidelity of repair of radiation damage. *Radiat. Prot. Dosimetry* **99**, 117–122 (2002).
70. V. A. Semenenko, R. D. Stewart and E. J. Ackerman, Monte Carlo simulation of base and nucleotide excision repair of clustered DNA damage sites. I. Model properties and predicted trends. *Radiat. Res.* **164**, 180–193 (2005).
71. V. A. Semenenko and R. D. Stewart, Monte Carlo simulation of base and nucleotide excision repair of clustered DNA damage sites. II. Comparisons of model predictions to measured data. *Radiat. Res.* **164**, 194–201 (2005).
72. D. J. Brenner, Track structure, lesion development, and cell survival. *Radiat. Res.* **124**, S29–S37 (1990).
73. R. K. Sachs, A. M. Chen and D. J. Brenner, Review: proximity effects in the production of chromosome aberrations by ionizing radiation. *Int. J. Radiat. Biol.* **71**, 1–19 (1997).
74. R. K. Sachs, D. J. Brenner, A. M. Chen, P. Hahnfeldt and L. R. Hlatky, Intra-arm and interarm chromosome intrachanges: Tools for probing the geometry and dynamics of chromatin. *Radiat. Res.* **148**, 330–340 (1997).
75. U. Amaldi and G. Kraft, Radiotherapy with beams of carbon ions. *Rep. Prog. Phys.* **68**, 1861–1882 (2005).
76. T. Kanai, N. Matsufuji, T. Miyamoto, J. Mizoe, T. Kamada, H. Tsuji, H. Kato, M. Baba and H. Tsujii, Examination of GyE system for HIMAC carbon therapy. *Int. J. Radiat. Oncol. Biol. Phys.* **64**, 650–656 (2006).